

Copyright © 1995, by the author(s).
All rights reserved.

Permission to make digital or hard copies of all or part of this work for personal or classroom use is granted without fee provided that copies are not made or distributed for profit or commercial advantage and that copies bear this notice and the full citation on the first page. To copy otherwise, to republish, to post on servers or to redistribute to lists, requires prior specific permission.

**EXPERIMENTAL MODELING OF A TRAVELING-
WAVE-EXCITED INDUCTIVELY DRIVEN COIL
FOR A LARGE AREA PLASMA SOURCE FOR
FLAT PANEL PROCESSING**

by

Yaoxi Wu and Michael A. Lieberman

Memorandum No. UCB/ERL M95/60

23 August 1995

COVER PAGE

**EXPERIMENTAL MODELING OF A TRAVELING-
WAVE-EXCITED INDUCTIVELY DRIVEN COIL
FOR A LARGE AREA PLASMA SOURCE FOR
FLAT PANEL PROCESSING**

by

Yaoxi Wu and Michael A. Lieberman

Memorandum No. UCB/ERL M95/60

23 August 1995

ELECTRONICS RESEARCH LABORATORY

College of Engineering
University of California, Berkeley
94720

**EXPERIMENTAL MODELING OF A TRAVELING-WAVE-EXCITED
INDUCTIVELY DRIVEN COIL FOR A LARGE AREA PLASMA
SOURCE FOR FLAT PANEL PROCESSING**

Yaoxi Wu¹ and Michael A. Lieberman²

¹Department of Materials Science and Engineering

and

²Department of Electrical Engineering and Computer Sciences

University of California, Berkeley CA 94720

Abstract

When the dimension of the antenna coil of an RF-powered plasma processing system is comparable to the RF wavelength, such as in a large area plasma source, the nonuniformity of power distribution due to the standing wave effect becomes intolerable. This is especially true for inductive coupled systems used for flat panel processing. To overcome this difficulty, a novel inductively-driven coil configuration coupled with a tuning network is proposed to launch a pure traveling wave on the coil, hence eliminating the standing wave effect. The configuration and scheme for driving the coil are illustrated by both theoretical analysis and experimental modeling. It is demonstrated that relatively uniform voltage amplitude profiles can be achieved for various system conditions by appropriately adjusting the tuning network. Under the tuned conditions, the

profiles only decay weakly (exponentially) along the coil due to the power consumption. The possibility of optimizing the uniformity of the attenuated voltage profiles using a small admixture of standing waves is shown.

I. Introduction

For large area substrate processing like manufacturing flat panels, a large area plasma source with low pressure and high density is required. Planar coil, inductively coupled plasma systems are known for their capabilities in generating a high plasma density under low pressure, and for their independent control of ion flux and ion-bombarding energy. With a planar coil configuration, a large area plasma source with a density as high as $10^{12}/\text{cm}^3$ has been reported[1]. These properties are favorable for increasing processing speed and minimizing contamination and substrate damage. As the plasma source becomes larger, however, a high uniformity becomes inherently more difficult to achieve. Among the many factors that influence the uniformity of the plasma source, the effect of standing waves along the exciting coil is crucial when the coil dimension is comparable to the wavelength of the RF driving source. Because flat panel processing requires a deposition uniformity $\leq \pm 5\%$ over large substrate areas for each film[2], the standing wave effect in a conventionally driven planar coil system for such an application will be intolerable. The standing wave formed in the coil causes the power dissipation to change dramatically along conducting windings comprising the coil, which leads to a nonuniform plasma density. In a conventionally driven inductive plasma source, the standing wave pattern may also depend on the plasma conditions and coil configuration, and may change from one process to another. To overcome these difficulties, a novel plasma processing system with a planar coil embedded in

the plasma and driven with an RF traveling wave is proposed. The coil in such a system is driven through a tuning network that can change the standing wave ratio as desired, independent of the matching network, which is used to match the RF power supply to the coil system. Theoretical analysis has been performed for this new configuration. An experimental model has been constructed and tested to verify the feasibility of eliminating the standing wave effect.

II. Theoretical Analysis of the Plasma and Coil Systems

The system under study is an inductive or transformer-coupled plasma system, with a planar coil configuration, designed for processing large area substrate such as flat panels or large size wafers. In a so-called transformer-coupled system, the inductive coil or transmission line driving the system acts like a primary coil and the plasma acts like a lossy secondary coil in a transformer. The system circuit diagram is sketched in Figure 1, and consists of four subsystems, namely, an RF power generator (a), a matching network (b), a tuning network (c), and an inductive coil or an antenna coil (d). The antenna coil is embedded in a rectangular processing chamber made of stainless steel with an inner dimension of 72.52×62.33×28.55 cm. The system may provide a plasma volume large enough to study the processing of silicon wafers as large as 300 mm in diameter and flat panel glass substrate sizes as large as 360 mm × 465 mm. The inductive coil layout inside the processing chamber consists of eight parallel copper tubes in series, with each of them covered with a quartz tube, as shown schematically in Figure 2. This coil configuration is specially designed to launch a traveling wave, and is quite different, not only in geometry but also in driving mechanism, from those with a spiral coil configuration reported in other

studies[1][3]–[6], where the field distribution inside the processing chamber is inherently nonuniform. Figure 3 shows the detailed structure and geometry of the primary coil and its coupling to the plasma. This coil-plasma system can be modeled as a transmission line, from which, the transmission line characteristic parameters can be evaluated. Its equivalent circuit is shown in Figure 4a. The characteristics of transformer-coupling are clearly illustrated.

The inductance matrix for this transformer coupled system may be define through the equations[7]

$$\tilde{V}_{rf} = j\omega L_{11}\tilde{I}_{rf} + j\omega L_{12}\tilde{I}_p \quad (1)$$

$$\tilde{V}_p = j\omega L_{21}\tilde{I}_{rf} + j\omega L_{22}\tilde{I}_p, \quad (2)$$

and the corresponding circuit diagram for these equations is shown in Figure 4b, where the inductances, capacitance and resistance per unit length, L_{11} , L_{12} , L_{21} , L_{22} , L_e , C , and R_p , referring to the geometric diagram in Figure 3, may be evaluated as

$$L_{11} = \frac{\mu_0}{2\pi} \ln \frac{d-a}{a} \quad (3)$$

$$L_{12} = L_{21} = \frac{\mu_0}{2\pi} \ln \frac{d-a}{b+\delta} \quad (4)$$

$$L_{22} \equiv L_p = \frac{\mu_0}{2\pi} \ln \frac{d-b-\delta}{b+\delta} \quad (5)$$

$$C = \frac{C_1 C_2}{C_1 + C_2} \quad (6)$$

$$L_e = \frac{R_p}{v_{eff}} \quad (7)$$

$$R_p = \frac{1}{\sigma_{eff} \pi [(\delta + b)^2 - b^2]} \quad (8)$$

where a is the outer radius of the copper tube; b is the outer radius of the quartz tube; δ is the plasma skin depth; d is the center distance between two neighbouring copper tubes; v_{eff} is the effective electron-neutral collision frequency, including both stochastic and ohmic heating effects; σ_{eff} is the effective plasma conductivity; and C_1 and C_2 are the effective capacitances per unit length of the air gap and quartz, respectively, which may be evaluated as follows

$$C_1 = \frac{2\pi\epsilon_0}{\ln\left(\frac{b-t}{a}\right)} \quad (9)$$

$$C_2 = \frac{2\pi\epsilon_0\epsilon_r}{\ln\left(\frac{b}{b-t}\right)} \quad (10)$$

where t is the quartz tube thickness. The resistance per unit length R_p accounts for the power dissipation in the plasma, and the inductance per unit length L_e accounts for the additional energy storage in the plasma due to the electron inertia[8]. The transmission line shown in Figure 4a may be reduced to that shown in Figure 4c with the corresponding characteristic parameters given by

$$Z_s = R_s + j\omega L_s = j\omega L_{11} + \frac{\omega^2 L_{12}^2}{R_p + j\omega(L_p + L_e)} \quad (11)$$

or

$$R_s = \frac{\omega^2 L_{12}^2 R_p}{R_p^2 + \omega^2 (L_p + L_e)^2} \quad (12)$$

$$L_s = L_{11} - \frac{\omega^2 (L_p + L_e) L_{12}^2}{R_p^2 + \omega^2 (L_p + L_e)^2} \quad (13)$$

This leads to the transmission line characteristic impedance

$$Z_0 = R_0 + jX_0 = \frac{\sqrt{2}}{2\sqrt{\omega C}} \left(\sqrt{\sqrt{(\omega L_s)^2 + R_s^2} + \omega L_s} + j\sqrt{\sqrt{(\omega L_s)^2 + R_s^2} - \omega L_s} \right), \quad (14)$$

admittance

$$Y_0 = G_0 + jB_0 = \frac{\sqrt{2}}{2} \frac{\sqrt{\omega C}}{\sqrt{R_s^2 + (\omega L_s)^2}} \left(\sqrt{\sqrt{(\omega L_s)^2 + R_s^2} + \omega L_s} + j\sqrt{\sqrt{(\omega L_s)^2 + R_s^2} - \omega L_s} \right), \quad (15)$$

and complex wave propagation constant

$$\gamma = \alpha + j\beta = \frac{\sqrt{2}}{2} \sqrt{\omega C} \left(\sqrt{\sqrt{(\omega L_s)^2 + R_s^2} - \omega L_s} + j\sqrt{\sqrt{(\omega L_s)^2 + R_s^2} + \omega L_s} \right), \quad (16)$$

where $\omega = 2\pi f$ is the angular frequency of the RF source.

A typical plasma environment of the system may be specified with the following parameters:

$a=0.635$ cm, $b=1.27$ cm, $d=7.62$ cm, $f=13.56$ MHz, $p=5$ mtorr, $n_g=1.7 \times 10^{14}$ cm⁻³, $n_s=10^{11}$ cm⁻³, $v_m=1.4 \times 10^7$ s⁻¹, $v_{stoc}=1.1 \times 10^7$ s⁻¹, $\sigma_{eff}=112.5$ $\Omega^{-1}\text{m}^{-1}$, $\delta=1.68$ cm, where p is the gas pressure; n_g is

the gas density; n_s is the plasma density; ν_m is the electron-neutral momentum transfer frequency; ν_{stoc} is the stochastic collision frequency, and σ_{eff} is the effective plasma conductivity. Equations (3) through (16) with these parameters yield transmission line characteristic parameters shown in Table 1. For a detailed evaluation procedure, please see 12.1 of monograph [9].

The voltage waveform of a sinusoidal signal on the transmission line for the plasma processing system may be written as follows

$$V = V_+ e^{-\gamma z} + \rho V_+ e^{\gamma z} \quad (17)$$

where V is the voltage distribution along the transmission line; V_+ , the voltage amplitude of the forward traveling wave; ρV_+ , the voltage amplitude of the backward traveling wave; ρ , the reflection coefficient; $\gamma = \alpha + j\beta$, the complex wave propagation constant; α , the attenuation constant; and β , the wave propagation constant. Clearly, when $\rho=0$, the wave is a pure traveling wave. To illustrate how the reflection coefficient influences the field distribution along the transmission line, i.e., the standing wave effect, the normalized voltage amplitude against the position in the transmission line with reflection coefficient as a parameter is plotted in Figure 5. It shows that a high wave reflection coefficient causes the field distribution along the transmission line to be extremely nonuniform, and that when the wave reflection coefficient is equal to zero, i.e., when the wave is a pure traveling wave, the best uniformity in field distribution is obtained. In a conventional plasma processing system, however, this situation is not achieved, since there is no way both to eliminate the backward traveling wave and to match the system impedance to that of power generator at same time. The reflection coefficient ρ varies

with the plasma conditions, and a small reflection, say, $\rho=0.2$, may cause a significant nonuniformity, as clearly shown in Figure 5. With a tuning network coupled into the proposed system as shown in Figure 1, and adjusted corresponding to the plasma conditions, a pure traveling wave can be achievable. This is illustrated in the following theoretical reasoning and the experimental modeling in the following section.

A circuit model for the system coupled with a tuning network for this analysis is sketched in Figure 6, where the X_1 and X_2 are the tuning elements. There are other ways to construct a tuning network; the one presented here is designed to obtain the symmetry between the forward and backward traveling waves, so as to, as will be seen latter, provide an easy way to control the standing wave ratio for studying the standing wave effect. With the origin of coordinate system chosen as indicated in Figure 6 and X_1 and X_2 treated as lumped elements, the voltage and current waveforms may be written as

$$V(z) = V_0 e^{-(\alpha+j\beta)z} + V_0 \rho e^{(\alpha+j\beta)z} \quad (18)$$

$$I(z) = Y_0 (V_0 e^{-(\alpha+j\beta)z} - \rho V_0 e^{(\alpha+j\beta)z}) \quad (19)$$

with the boundary condition

$$V(\pm d) = V_0 e^{\mp(\alpha+j\beta)d} + \rho V_0 e^{\pm(\alpha+j\beta)d} = V_{2,1} \quad (20)$$

$$I(\pm d) = Y_0 (V_0 e^{\mp(\alpha+j\beta)d} - \rho V_0 e^{\pm(\alpha+j\beta)d}) = I_{2,1} \quad (21)$$

and the relation according to Kirchhoff's law

$$V_2 = Z_1 I_1 + V_1 + Z_2 I_2, \quad (22)$$

where l is the length of transmission line; $d = l/2$, $Z_1 = j X_1$ and $Z_2 = j X_2$; V_0 is the amplitude of the forward traveling wave; Y_0 is the admittance of the transmission line as defined through Eqn. (15); and ρ is the reflection coefficient, which, in general, is a complex number and may be written as

$$\rho = \rho_r + j\rho_i \quad (23)$$

This complex linear system is solved analytically and the reactances of tuning elements X_1 and X_2 are obtained as follows

$$X_1 = [2\rho_i B_0 + G_0(\rho_r^2 + \rho_i^2 - 1)] \frac{\cos\beta l}{D} - B_0[(\rho_r - 1)^2 + \rho_i^2] \frac{\sin\beta l}{D} + [G_0(1 - \rho_r) - \rho_i B_0] \frac{e^{-\alpha l}}{D} - [G_0(\rho_r^2 + \rho_i^2) + \rho_i B_0 - \rho_r G_0] \frac{e^{\alpha l}}{D} \quad (24)$$

$$X_2 = [2\rho_i B_0 + G_0(\rho_r^2 + \rho_i^2 - 1)] \frac{\cos\beta l}{D} + B_0[(\rho_r - 1)^2 + \rho_i^2] \frac{\sin\beta l}{D} + [G_0(1 - \rho_r) - \rho_i B_0] \frac{e^{\alpha l}}{D} - [G_0(\rho_r^2 + \rho_i^2) + \rho_i B_0 - \rho_r G_0] \frac{e^{-\alpha l}}{D} \quad (25)$$

where

$$(B_0^2 + G_0^2) [\rho_i(e^{-\alpha l} - e^{\alpha l}) + (\rho_r^2 + \rho_i^2 - 1)\sin\beta l] \quad (26)$$

and where G_0 and B_0 are characteristic conductance and susceptance of the transmission line as defined through Equation (15), and α and β are the wave attenuation and propagation constants respectively, as defined through Equation (16). X_1 and X_2 may be capacitive, if they are smaller than zero, or inductive, if they are larger than zero. For a specific system, with the characteristic parameters given, Eqns. (24) and (25) give the relation between the reactances of the tuning elements X_1 and X_2 and the reflection coefficient.

The conditions for obtaining a pure traveling wave are specified by

$$\rho_r = \rho_i = 0 \quad (27)$$

in Eqns. (24) and (25), which lead to

$$X_1 = \frac{-G_0 e^{-\alpha l} + (B_0 \sin \beta l + G_0 \cos \beta l)}{(B_0^2 + G_0^2) \sin \beta l} \quad (28)$$

$$X_2 = \frac{-G_0 e^{\alpha l} - (B_0 \sin \beta l - G_0 \cos \beta l)}{(B_0^2 + G_0^2) \sin \beta l} \quad (29)$$

These two equations give the required reactances of elements X_1 and X_2 to achieve a pure traveling wave along the coil. The reactances of X_1 and X_2 against R_s , the transmission line resistance per unit length, which, in a processing system, depends on the plasma conditions, are plotted according to Eqns. (27) and (28) in Figure 7 for a few different transmission line lengths. Figure 7 implies that whenever a change in plasma conditions occurs, X_1 and X_2 may be adjusted accordingly to ensure a pure traveling wave in the transmission line. The figure also shows that

under typical plasma operating conditions, $R_s = 1-3 \Omega$, and for the desired length of transmission line in our system, $l=8-9.5$ m, the tuning elements X_1 and X_2 remain inductive; hence, practically, a tuning network with two inductors only is capable of appropriate adjustment. This is one of the advantages of this tuning network configuration. The fact that X_1 and X_2 are equal at $R_s=0$ indicates that if there is no power dissipation in the system, a pure traveling wave would be unachievable—due to the symmetry, the tuning system would not favor a wave traveling in one direction over another.

Though not desirable in a practical system, it may be of theoretical interest to see the conditions for obtaining a pure standing wave. Since a pure standing wave means that the forward and backward waves have the same wave amplitude, one may expect, in light of the symmetry of the system, that $X_1=X_2$. This is indeed the case. By specifying

$$\rho_r = 1, \quad \rho_i = 0 \quad (30)$$

in Eqns. (23) and (24), we obtain

$$X_1 = X_2 = \frac{2G_0 \cos \beta l - G_0 (e^{-\alpha l} + e^{\alpha l})}{2(B_0^2 + G_0^2) \sin \beta l} \quad (31)$$

It is worthwhile to mention that since both the tuning network and the exciting coil are symmetric, the X_1 and X_2 are commutable, which means that forward and backward traveling waves are arbitrary defined, and that the tuning network is capable of launching a pure forward

or backward traveling wave, or a wave with any standing wave ratio. This provides a feasible way to experimentally study the relation between standing wave ratio, system configuration and plasma conditions. This can be illustrated using Eqns. (24) and (25). The inductances of X_1 and X_2 against R_s for $l = 8.9$ m are plotted from Eqns. (24) and (25) in Figure 8, with the reflection coefficient as a parameter. For simplicity, we have specified that $\rho_i=0$ and plotted X_1 and X_2 with $\rho=\rho_r=0, 0.2, 0.5, 0.8$ and 1 respectively. Figure 8 shows how easily X_1 and X_2 can be adjusted to achieve different standing wave ratios. This is another advantage of this tuning network configuration. Under the pure traveling wave condition, i.e., $\rho=0$, X_1 and X_2 has a maximum separation. As ρ increases, i.e., as the situation approaching the pure standing wave condition, X_1 decreases and X_2 increases and the separation between them becomes smaller. They coincide at $\rho=1$, which corresponds to the pure standing wave condition. Again we see that for the pure standing wave condition, $X_1=X_2$. A further decrease in X_1 and increase in X_2 will make the situation repeat itself, but with the backward traveling wave dominating, until a pure backward traveling wave is obtained at the point where X_1 and X_2 exchange their original positions.

III. Experimental Results on a Simulation Model System

As may be seen from the discussion so far, in an inductively coupled plasma processing system, the driving coil plus plasma itself can be treated as a lossy transmission line. The plasma represents a power consumption component, equivalent to a transmission line resistance, and the value of the resistance corresponds to different plasma conditions. Implementing this reasoning, we have constructed, as shown in Fig. 9, a model system with resistors in series with the outer conductors of coaxial cables. In the model system, the copper tubes in the plasma processing

chamber in figure 2 are replaced by eight RG 312/U coaxial cables with characteristic capacitance $C=101$ pF/m and impedance $Z=50\Omega$. A $2\text{-}\Omega$ high frequency resistor is connected in series with the outer shields of each of the eight coaxial cables, which yields the line characteristic parameters as summarized in Table 1. It is seen that the experimental model system has similar characteristics to those of the real plasma system. It is worthwhile to mention that no effort has been taken to make the characteristic parameters identical in the two systems—they should be similar, but not necessary identical, since the main purpose of this study is to demonstrate the feasibility of launching a pure traveling wave in order to improve the plasma uniformity. It is easy in a model system like ours, by adjusting the value of the resistors and the length of the transmission line, to simulate various system situations that otherwise may be costly to achieve experimentally in a real plasma processing system. The tuning network consists of two identical coil inductors with a variable range from 215 nH to 14 μ H. A wattmeter is connected in series in the middle of the transmission line to monitor the forward and backward powers. Two variable capacitors, with adjustable ranges of 22 pF to 1000 pF and 45 pF to 1800 pF respectively, serve as the matching network to ensure an impedance matching between the RF power supply and the rest of the system.

By adjusting the tuning elements X_1 and X_2 , we have observed the complete disappearance of the backward or forward traveling wave under various conditions. In each experiment, the dial readings of the variable inductors for each disappearance of backward or forward traveling waves were recorded. The experiments were performed for a few different resistances and transmission line lengths. After the experimental measurements, the tuning network was connected to an HP

8753A RF network analyzer to obtain the reactances of X_1 and X_2 corresponding to each pair of dial readings. The results are plotted in Figure 10 along with the corresponding curves from a theoretical evaluation from Eqns. (27) and (28). It is seen that the agreement between the theoretical analysis and experimental modeling is reasonable. Since the tuning system is symmetric, as mentioned above, the tuning conditions for the forward traveling waves only are plotted.

The experiments for the tuning conditions vs. different driving frequencies were also performed in a similar manner. The experimental results and corresponding theoretical evaluation are plotted in Figure 11 for a line length $l= 8.9$ m, and the agreement between them is surprisingly good. It was also found that when the operating frequency is beyond the range shown in Figure 11, we were unable to launch a pure traveling wave using a tuning network with two inductors. To understand why, we plotted, using the theoretical formulation presented in the previous section, the required values of X_1 and X_2 for launching a pure traveling wave for a wider frequency range, say, 8 MHz to 21 MHz, for $l=8.9$ m, and the results are shown in Figure 12. Note that X_1 and X_2 are indistinguishable in the figure due to the large vertical scale values. Figure 12 clearly shows that the values of the tuning elements needed for lower or higher operating frequency are beyond what we have in our current tuning network (215 nH–14 μ H). At low operating frequency capacitive elements are required, and at high frequency, smaller inductors. This further verifies our theoretical reasoning to predict the system behavior under the proposed plasma operating conditions.

After a pure traveling wave had been launched successfully, the matching network coupled into the system as shown in Figure 1 was adjusted to ensure the impedance matching between the power supply and the rest of the system. It was observed that the conditions of the matching network have a negligible influence on the tuning conditions.

To observe the standing wave effect experimentally, the experiments were also conducted to measure the voltage amplitude along the antenna coil. Nine voltage sampling ports (labeled # 1–9 in Fig. 9) were set up along the transmission line with a spacing of 0.98 m between two neighboring ports, except the last one (# 9) which has a distance of 0.6 m from the proceeding port. The peak to peak waveform amplitudes for each port were read by a HP 54503A digitizing oscilloscope. The tuning network is adjusted to obtain the desired wave reflection coefficient. The reflection coefficient ρ is calculated from the wattmeter readings of the forward and backward powers as follows

$$\rho = \sqrt{\frac{P_b}{P_f}} \quad (32)$$

where the P_b and P_f are the backward and forward power readings respectively. The results are plotted in Fig. 13 for a few different reflection coefficients and power readings. Since this preliminary experiment is set up to observe the standing wave effect only, and not for quantitative analysis, the power input for the measurement was arbitrary chosen. It can be seen

that the standing wave effect, which is quite significant, is clearly shown. The reason that we did not get a weak exponential decay at $\rho = 0$ for the voltage amplitude as shown in the theoretical analysis, may be due to the voltage drop caused by finite ground loop lengths which are different for each of the sampling ports. Under pure traveling wave conditions, the voltage difference between two neighboring ports is, according to the theoretical evaluation, very small, say, less than 2%. This figure may be comparable to the measuring uncertainty in the voltage.

IV. Further Investigation

If we examine Fig. 5 carefully, we will find that the average of a voltage amplitude profile always decreases slightly as the wave travels down the transmission line. Due to the power dissipation, a general tendency for this decrease in voltage amplitude is inevitable. The question then naturally arises, "can we alleviate the attenuation of voltage amplitude locally by means of the tuning network since our tuning network is capable of changing the standing wave ratio"? To answer this question, a computer simulation program was written based on a theoretical reasoning similar to that on which Eqns. (24) and (25) were derived. This program is capable of "probing" into any position along the transmission line and displaying the variation of the voltage with time, and of displaying the voltage amplitude along the transmission line. Using this program, we are also able to display how the voltage amplitude profile changes with the amplitude and phase of reflection coefficient. Figure 14 shows the simulation results for a reflection coefficient amplitude $\rho=0.02$, with the phase angle ϕ changing from π to $8/5\pi$. For comparison, the voltage amplitude of the pure traveling wave is also plotted. The improvement in voltage amplitude profile is evident at $\phi=6/5\pi$, compared with that of the pure traveling wave. This indicates that a pure

traveling wave does not always generate the best voltage amplitude profile, and that appropriately launching an essentially pure traveling wave superimposed with a backward traveling wave of a small amplitude may result in a better profile. For example, it may be desirable to have the voltage amplitude at edges of the processing chamber slightly larger than that at center to compensate for the low plasma density at edges due to particle diffusion. Though a complete compensation would be impossible according to our theoretical analysis, an improvement may be expected. This, fortunately, can be easily done experimentally by means of the tuning network. A future study will focus on achieving such a voltage amplitude profile in an experimental system, and on investigating the relation between plasma uniformity and voltage profile.

V. Concluding Remarks

An experimental model system for large area plasma sources has been used to investigate the possibility to obtain uniform voltage amplitude profiles. A tuning network was constructed and coupled into the system, which played a key role in launching a pure traveling wave. In such a tuning network configuration, only two variable inductors are required for the appropriate tuning for the plasma conditions of interest.

It has been proved theoretically and observed experimentally that a pure traveling wave can be launched under different experimental conditions by adjusting the inductances in the tuning network, corresponding to different plasma conditions. With this configuration, a processing system can be operated under a variety of plasma conditions while driven by a pure traveling wave. This can be easily done, in a practical plasma processing system, by either manual or

computer controlled adjustable tuning elements. It is expected that this will improve the uniformity of such plasma processing systems significantly. In addition, since the field profile in a traveling wave driven system is relatively independent of the exciting coil dimension, the system has favorable properties for scaling to larger sizes without much modification in the antenna design.

Moreover, the new system configuration has the capability to generate an RF wave with a desired standing wave ratio; this provides a convenient way to study the standing wave effect in a controllable manner.

Further improvement in voltage amplitude profiles has also been explored. Computer simulation suggests an approach to achieve this goal by locally regulating the voltage amplitude profile. In our system configuration, this can be easily done by means of the tuning network.

Acknowledgement

The authors would like to thank David Baca for his assistance in setting up the model experimental system and in preparing materials for the experiments. This work was partially supported by NSF Grant ECS-917500, DOE Grant DE-FG03-87ER13727, LLNL Grant W-7405-ENG-48, and a gift from Lam Research Corporation.

References

- [1] L.J. Mahoney, M.E. Wendt, E. Barrios, and C.J. Richards, *J. Appl. Phys.* 76 (4), 2041 (1994).
- [2] J.L. Crowley, *Solid State Technology*, 35(2), 94 (1992).
- [3] J. Hopwood, C.R. Guarnieri, S.J. Whitehair, and J.J. Cuomo, *J. Vac. Sci. Tech. A.* 11(1), 147 (1993).
- [4] R. Patrick, P. Schoenborn, H. Toda, and F. Bose, *J. Vac. Sci. Tech. A.* 11, 1296 (1993).
- [5] J.B. Carter, J.P. Holland, E. Peitzer, B. Richardson, E. Bogel, H.T. Nguyen, Y. Melaku, D. Gates, and M. Ben-Dor, *J. Vac. Sci. Tech. A.* 11, 1301 (1993).
- [6] P.L.G. Ventzek, R.J. Hoekstra, and M.J. Kushner, *J. Vac. Sci. Tech. A* 12, 461 (1994).
- [7] S.E. Schwarz and W.G. Oldham, *Electrical Engineering: An Introduction*, Holt, Rinehart & Winston, New York (1984).
- [8] R.B. Piejak, V.A. Godyak and B.M. Alexandrovich, *Plasma Sources, Sci. Tech.* 1, 179, (1992).
- [9] M.A. Lieberman and A. J. Lichtenberg, *Principles of plasma Discharges and Materials Processing*, John Wiley & Sons, New York (1994).

Figure and Table Captions

Figure 1. The circuit schematic of the Large Area Plasma Source system, with the tuning network shown to eliminate the standing wave effect. L_1 and L_2 are two identical variable inductors with an adjustable range from 215 nH to 14 μ H. (a) RF power generator; (b) matching network; (c) tuning network; (d) antenna coil.

Figure 2. Antenna coil system. The coil is made of a series of copper tubes, each covered by a quartz tube and embedded in the plasma.

Figure 3. The structure and geometry of the coil-plasma transmission line model; a is the outer radius of the copper tube; b is the outer radius of quartz tube; d is the center distance between two neighboring copper tubes; δ is the plasma skin depth; and t is the quartz tube thickness.

Figure 4. Equivalent circuit of the transmission line, showing transformer coupled plasma system; (a) coupled coil-plasma system; (b) transformer model; (c) equivalent transmission line.

Figure 5. Normalized voltage amplitude vs. the position along transmission line, with reflection coefficient ρ as a parameter, showing the standing wave effect on the field distribution along the transmission line.

Figure 6. Schematic circuit used to derive the tuning conditions, showing a forward traveling wave propagating along the transmission line.

Figure 7. The reactances of tuning elements X_1 and X_2 at tuned conditions vs. the transmission line resistance per unit length R_s for the line lengths $l=8.5$ m, 9.0 m, 9.5 m, from a theoretical evaluation.

Figure 8. The reactances of tuning elements X_1 and X_2 vs. the transmission line resistance per unit length with reflection coefficient ρ as a parameter, showing how X_1 and X_2 can be adjusted to obtain a wave with desired standing wave ratios.

Figure 9. Schematic of the experimental simulation model. The numbers indicate the locations of the voltage sampling ports.

Figure 10. Reactances of the tuning elements X_1 and X_2 at tuned conditions vs. resistance per unit length R_s , with transmission line length l as a parameter; solid lines are theoretical results; scattered points are experimental results.

Figure 11. Reactances of the tuning elements X_1 and X_2 at tuned conditions vs. driving frequency f for $l=8.9$ m. Solid lines are theoretical results; scattered points are experimental results.

Figure 12. Reactances of the tuning elements X_1 and X_2 at tuned conditions vs. driving frequency

f for $l=9$ m for a wider frequency range (8 MHz–21 MHz), from a theoretical evaluation.

Figure 13. Measured voltage amplitudes along the transmission line for a few different reflection coefficients, showing the standing wave effect experimentally, where P_f is the forward power and P_b is the backward power.

Figure 14. Voltage amplitude vs. position along the transmission line when a backward wave with a small amplitude is superimposed on the forward traveling wave. The reflection coefficient is $\rho=0$, and $\rho=0.02$ with the phase $\phi=\pi, 6/5\pi, 7/5\pi, 8/5\pi$.

Table 1. Comparison of typical transmission line characteristic parameters of the plasma system with those of the experimental model system.

Table 1

| | Plasma System | Modeling System |
|------------------------|-------------------------|--------------------------|
| C | 80.2 pF/m | 101 pF/m |
| L | 0.365 μ H/m | 0.247 μ H/m |
| R | 1.81 Ω /m | 1.80 Ω /m |
| Z (at $f=13.56$ MHz) | 67.51 -j 1.965 Ω | 50.4 - j 1.9992 Ω |
| α | 0.0134/m | 0.0168/m |
| β | 0.47/m | 0.426/m |

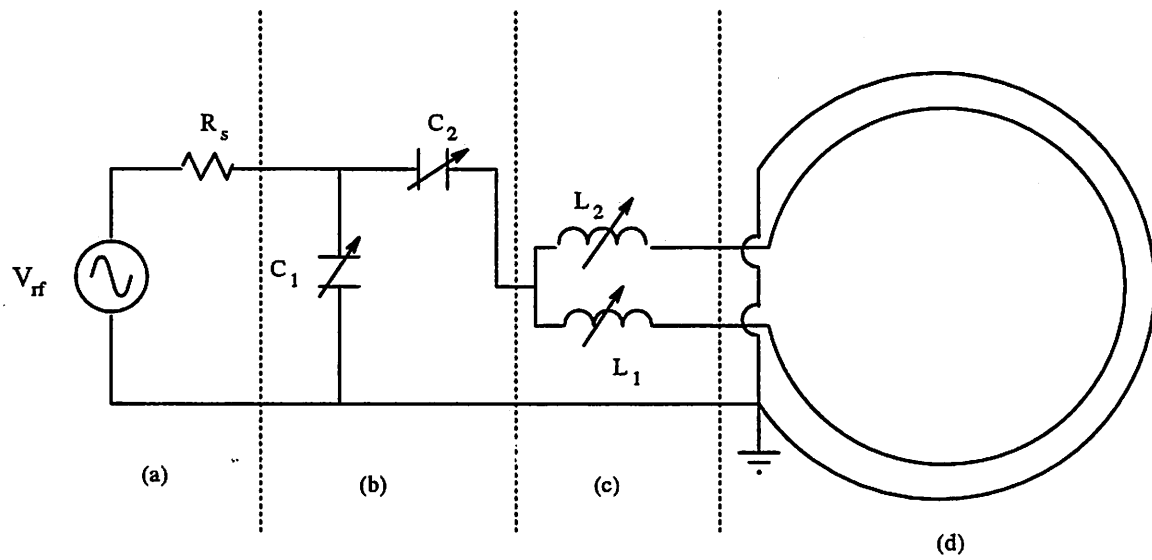


Figure 1

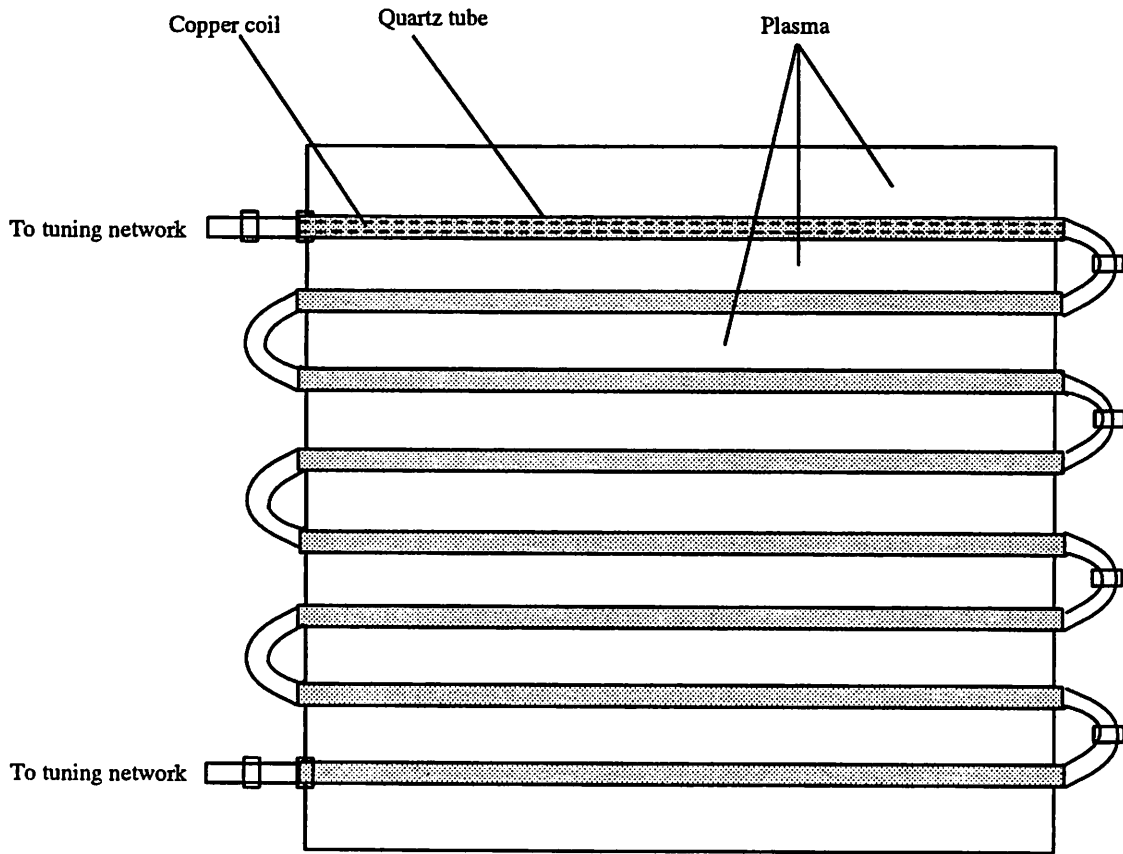


Figure 2

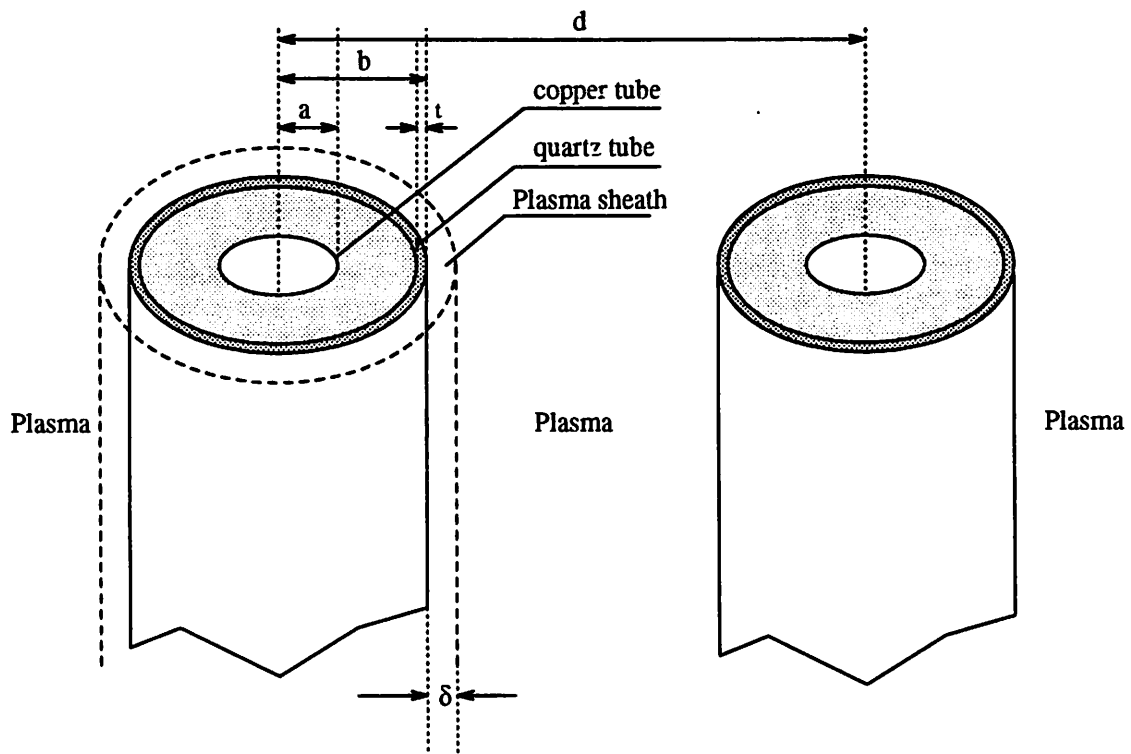
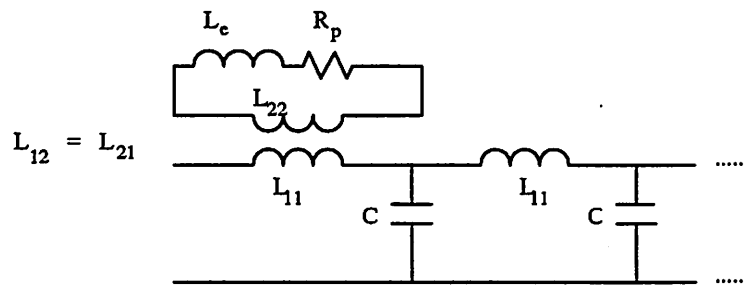
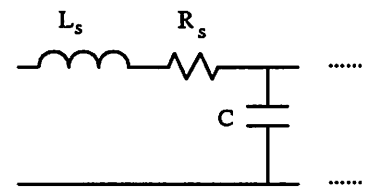


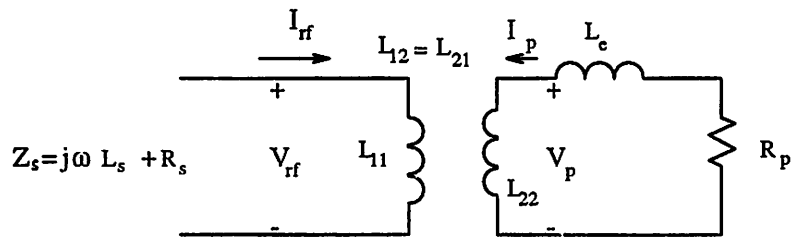
Figure 3



(a)



(c)



(b)

Figure 4

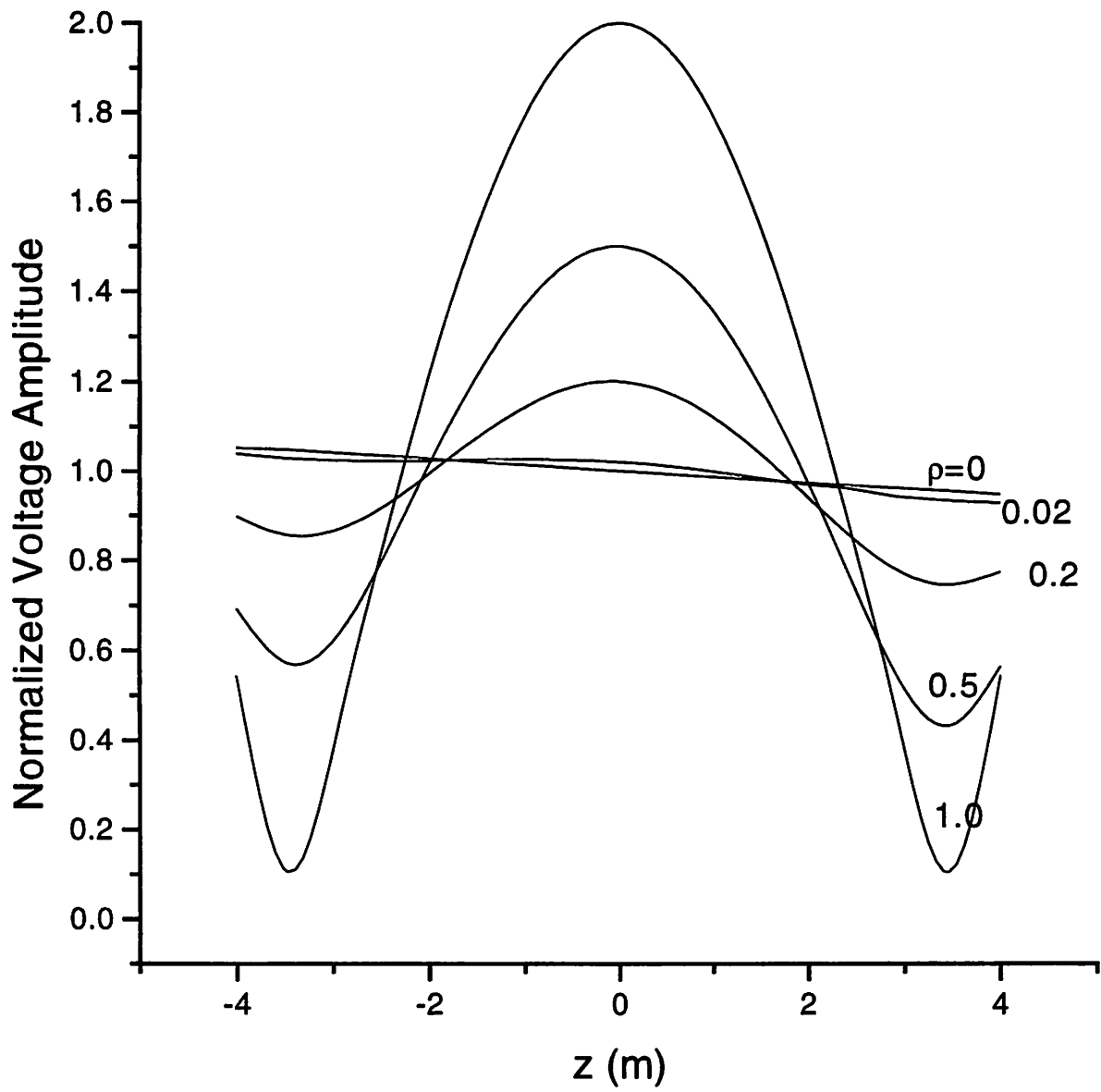


Figure 5

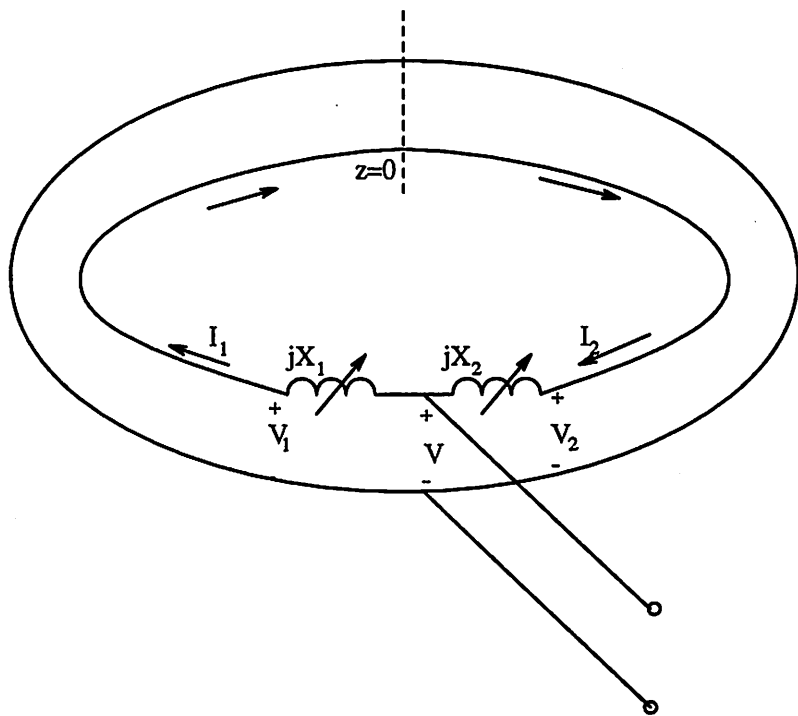


Figure 6

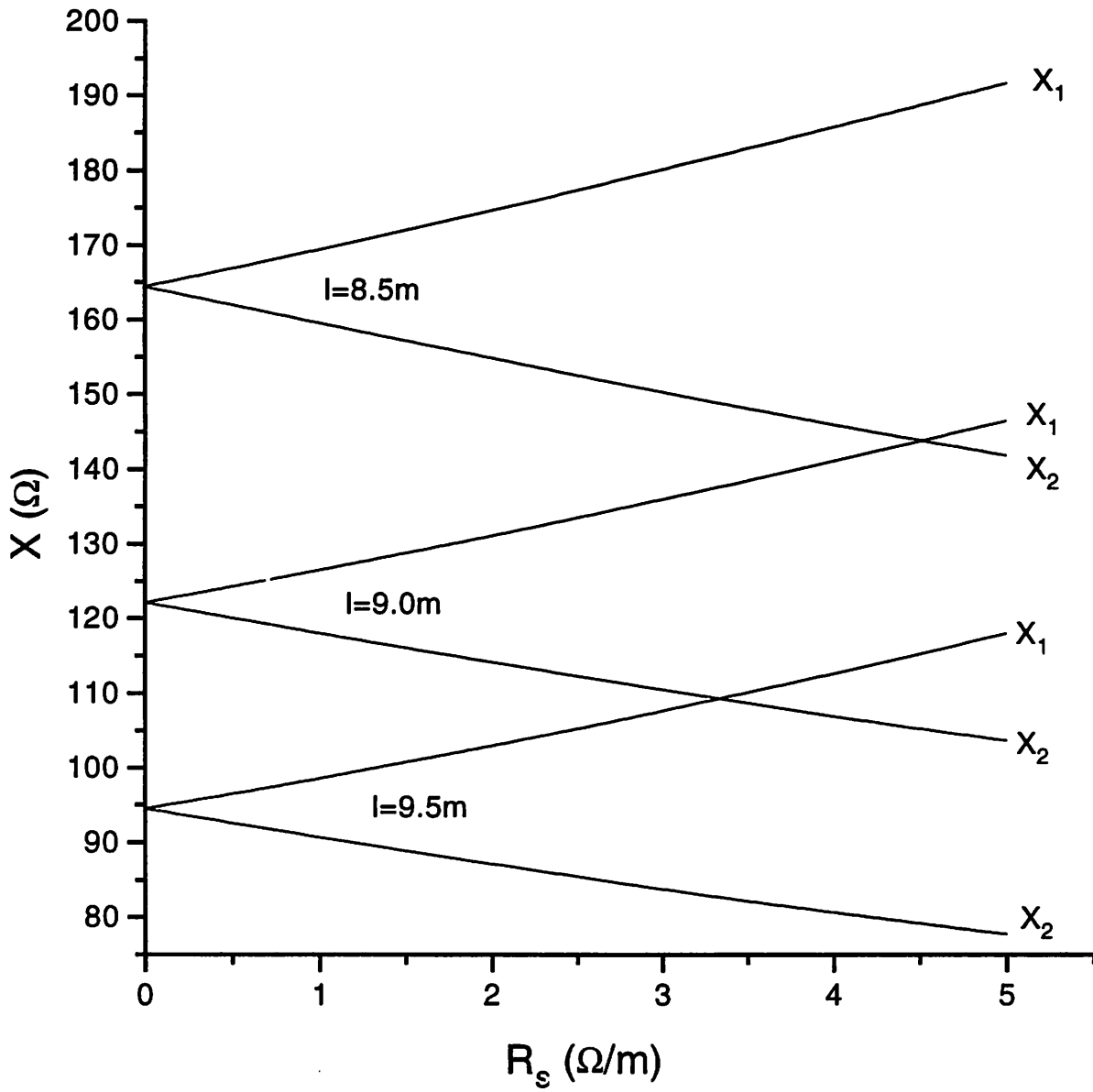


Figure 7

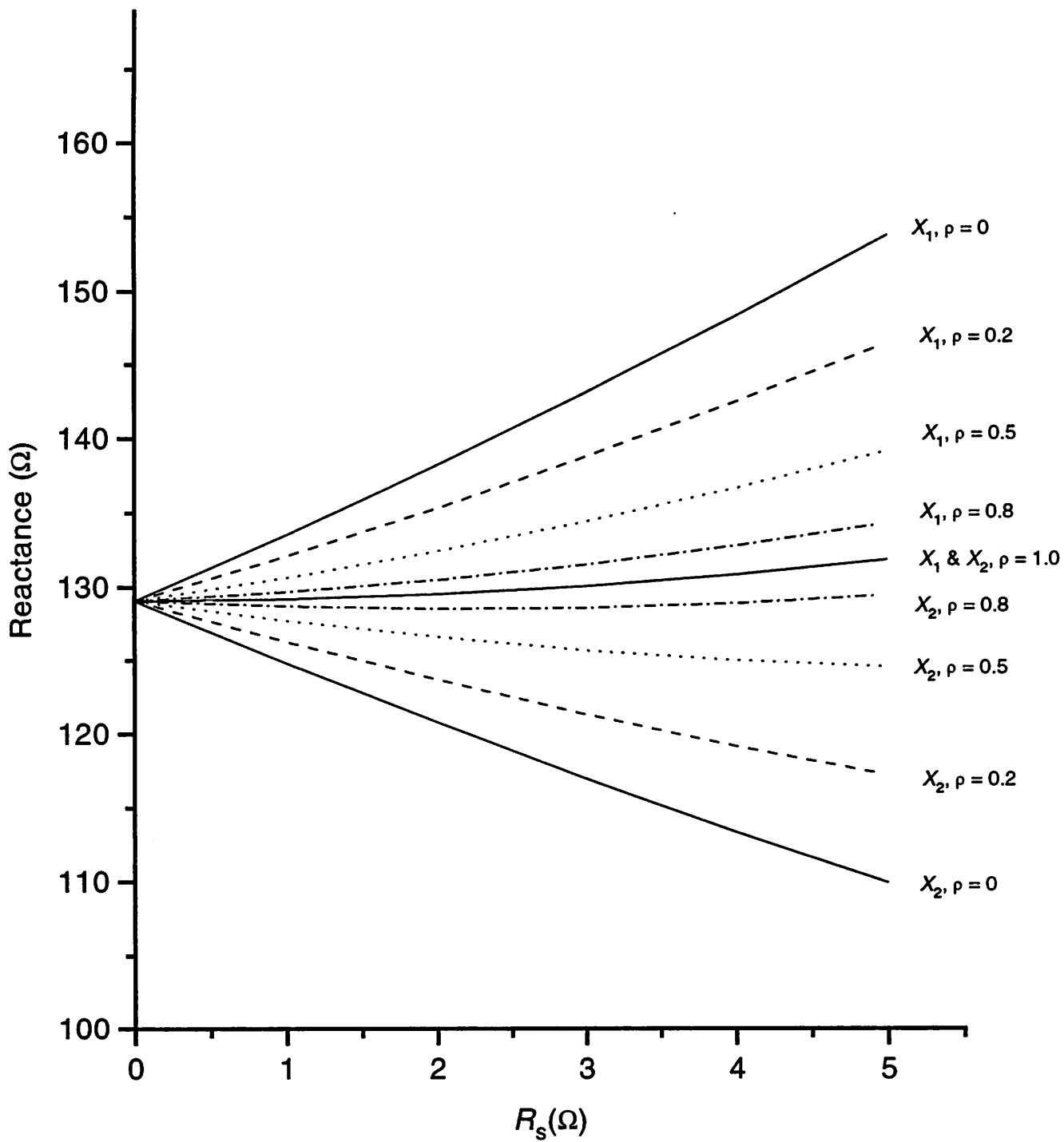


Figure 8

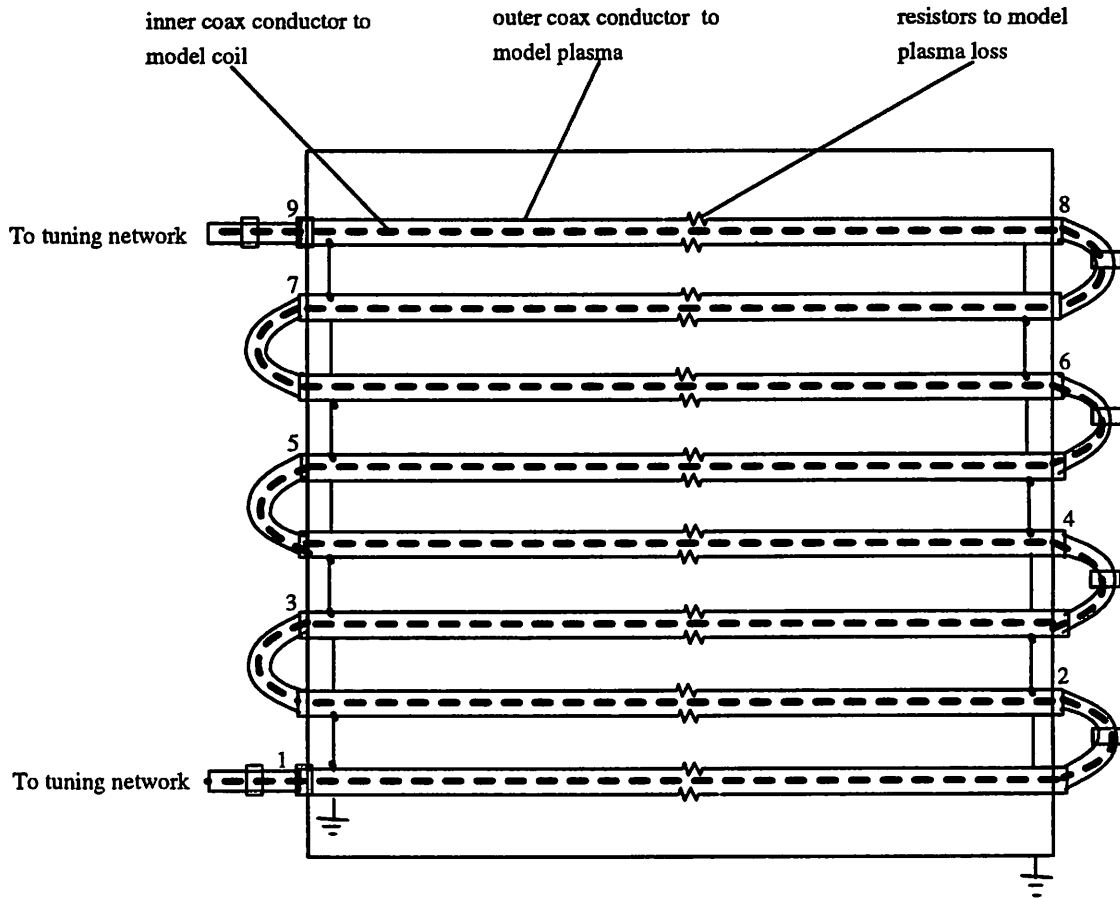


Figure 9

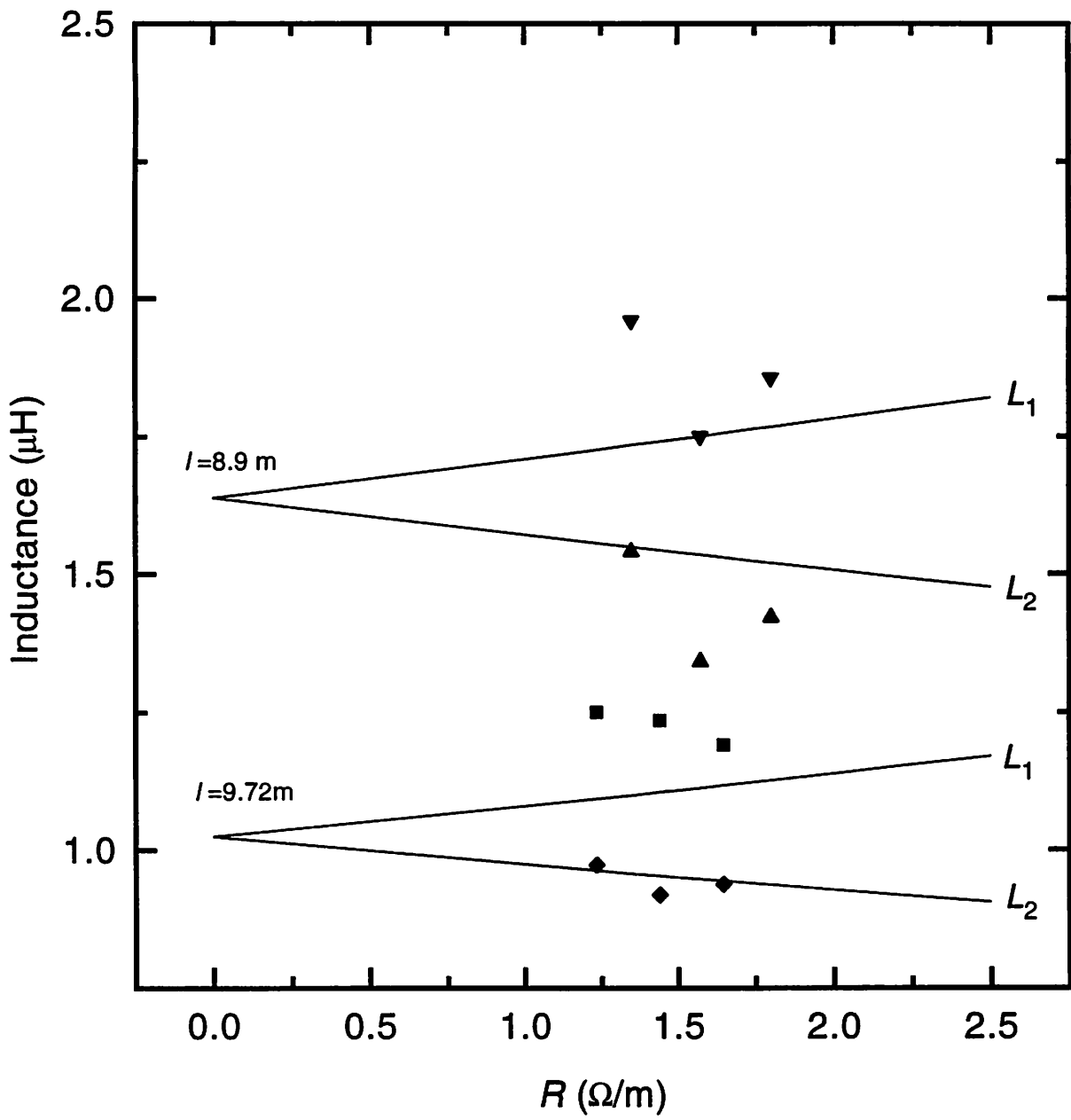


Figure 10

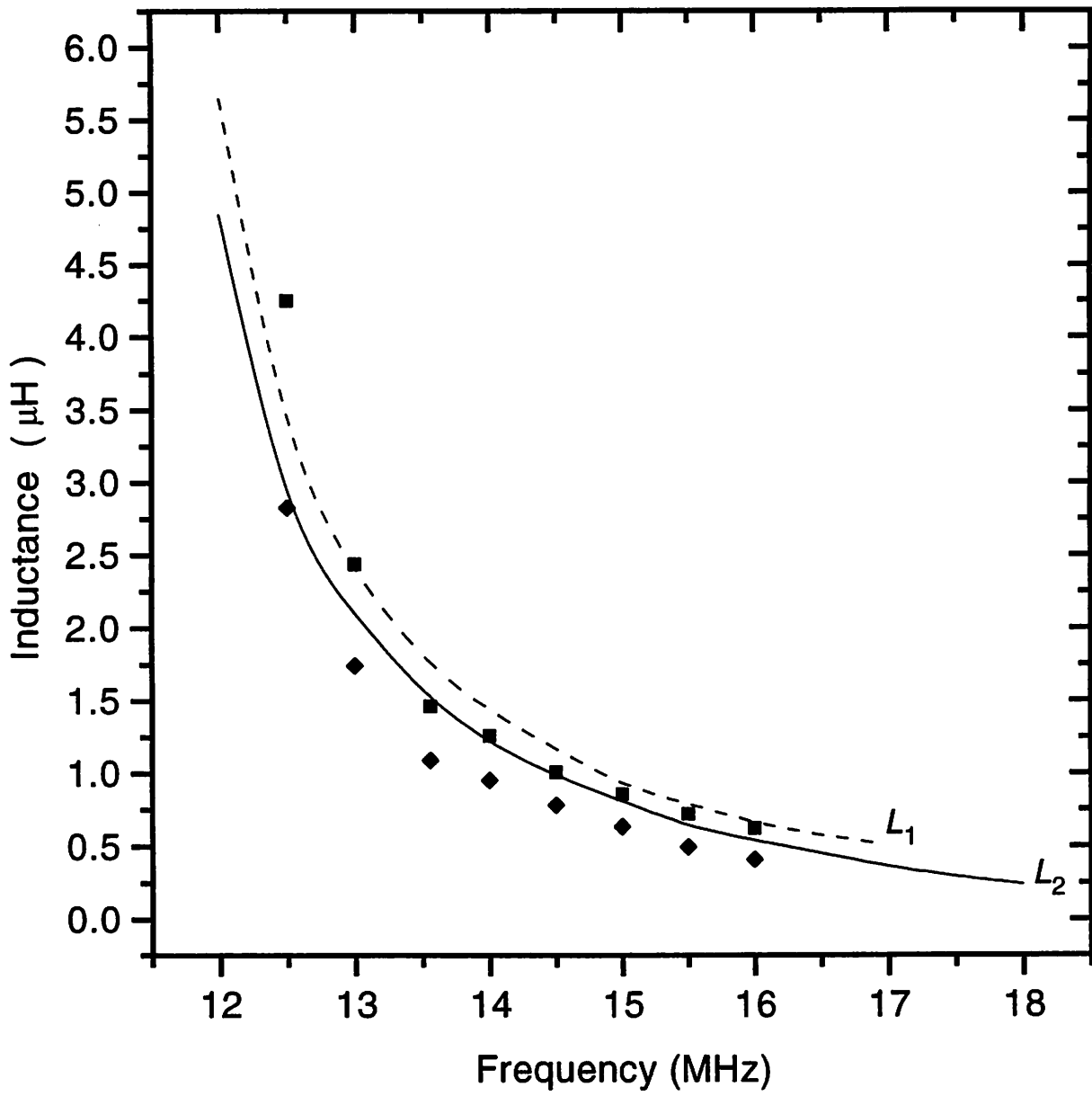


Figure 11

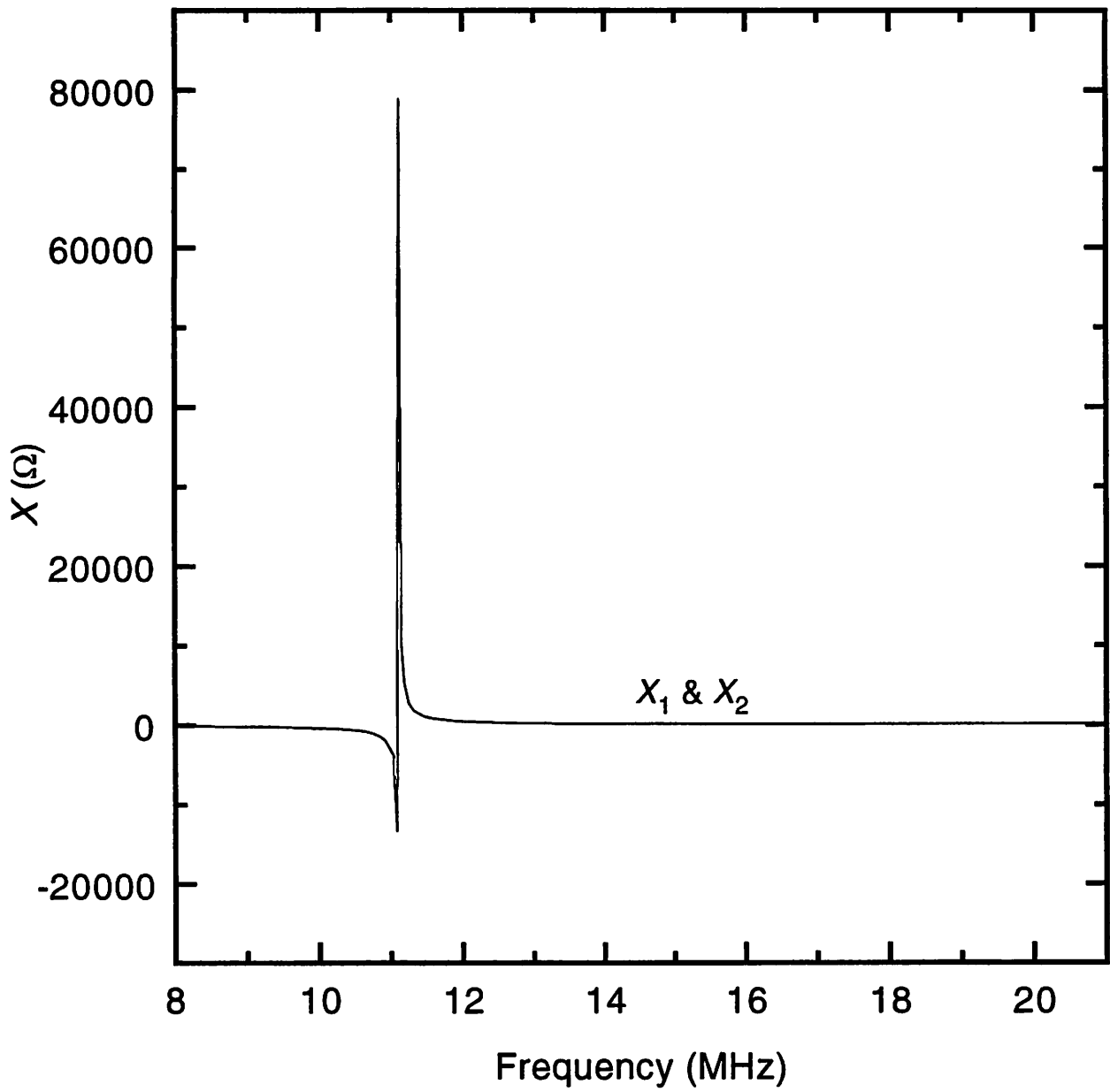


Figure 12

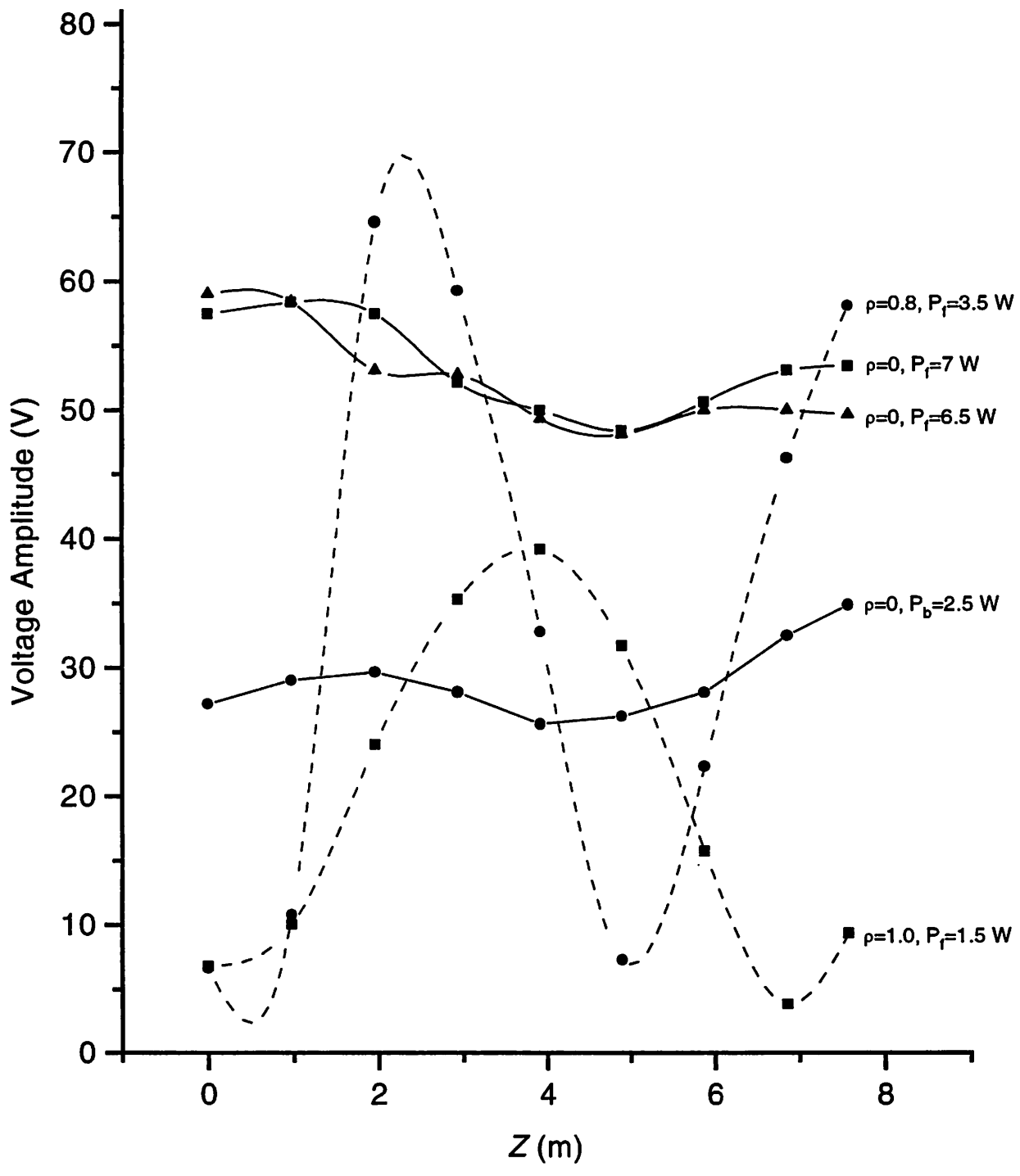


Figure 13

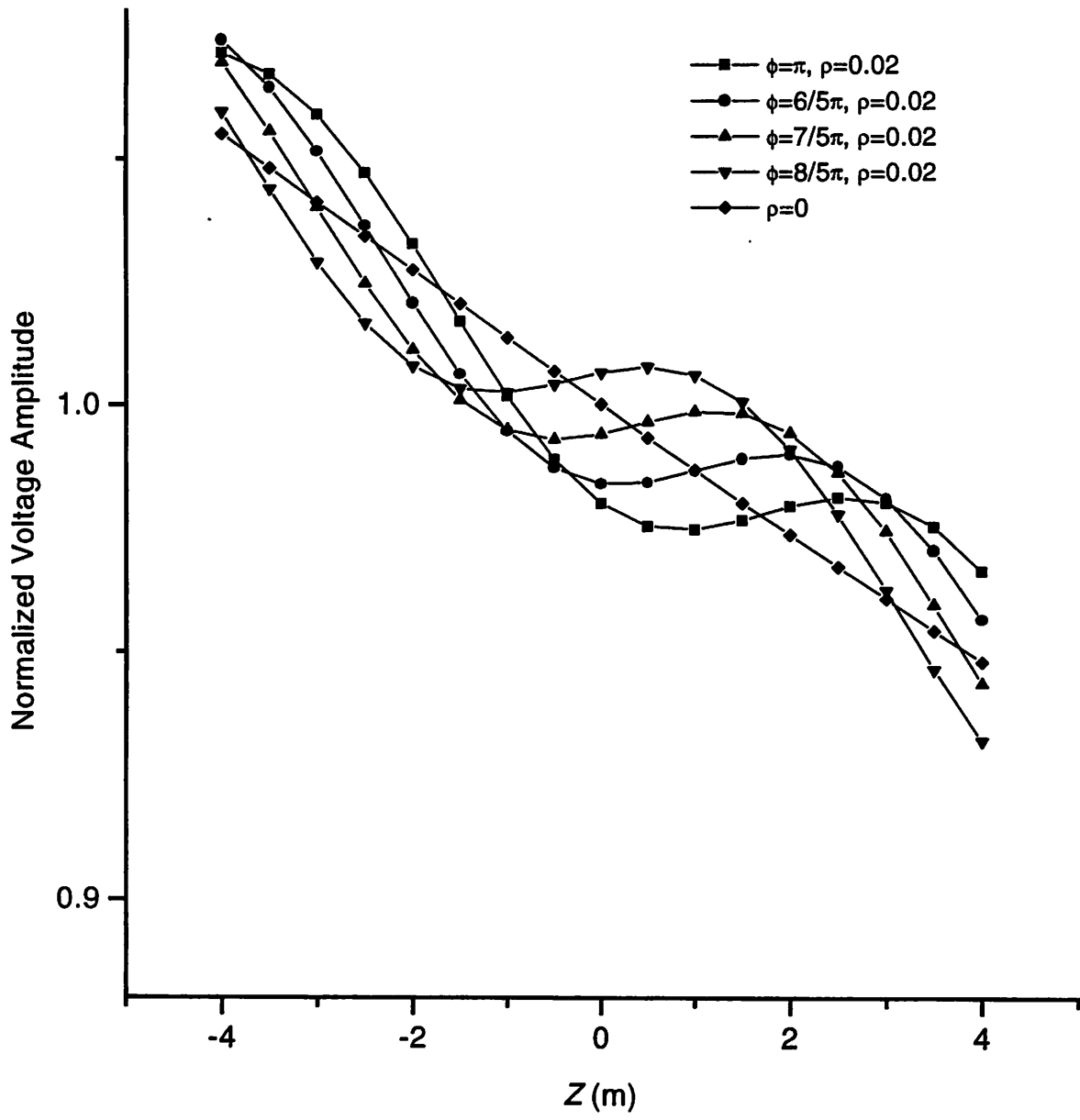


Figure 14